UC Berkeley
UC Berkeley Previously Published Works

Title
Correlations between Salt-Induced Crystallization, Morphology, Segmental Dynamics, and Conductivity in Amorphous Block Copolymer Electrolytes

Permalink
https://escholarship.org/uc/item/5gq469g4

Journal
Macromolecules, 51(5)

ISSN
0024-9297

Authors
Thelen, Jacob L
Wang, Andrew A
Chen, X Chelsea
et al.

Publication Date
2018-03-13

DOI
10.1021/acs.macromol.7b02415

Peer reviewed

Correlations between Salt-Induced Crystallization, Morphology, Segmental Dynamics, and Conductivity in Amorphous Block Copolymer Electrolytes

Jacob L. Thelen,[†,‡,§] Andrew A. Wang,[†] X. Chelsea Chen,[‡] Xi Jiang,[‡] Eric Schaible,[∥] and Nitash P. Balsara*[,†,‡,§,⊥]

[†]Department of Chemical and Biomolecular Engineering, University of California, Berkeley, Berkeley, California 94720, United States
[‡]Materials Sciences Division, [§]Joint Center for Energy Storage Research (JCESR), [∥]Advanced Light Source, and [⊥]Environmental Energy Technologies Division, Lawrence Berkeley National Laboratory, Berkeley, California 94720, United States

S *Supporting Information*

ABSTRACT: Block copolymer electrolytes have been shown to increase the cycle life of rechargeable batteries that utilize high capacity lithium anodes. Most block copolymer electrolyte studies have been centered on polystyrene-*b*-poly-(ethylene oxide) (SEO) mixed with lithium bis(trifluoro-methanesulfonyl)imide (LiTFSI) salt and are limited to salt concentrations in the vicinity of $r \equiv [\text{Li}]/[\text{EO}] = 0.1$, where [Li] and [EO] are the concentration of lithium and ethylene oxide moieties, respectively, as the conductivity of poly-

(ethylene oxide) (PEO) homopolymer electrolytes is maximized at this concentration. In this work, we study the morphology and conductivity of electrolytes derived from a high molecular weight SEO block copolymer over the wide LiTFSI concentration range of $0 \leq r \leq 0.550$. For electrolytes with $r \geq 0.125$, the crystallization of PEO−LiTFSI complexes with stoichiometric ratios of 6:1, 3:1, or 2:1 (EO:Li) is shown to correlate with morphology as determined by small-angle X-ray scattering (SAXS) and scanning transmission electron microscopy (STEM): some samples that are semicrystalline at room temperature exhibit regions of periodic lamellar ordering, whereas those that do not crystallize have aperiodic packed-ellipsoid morphologies. SAXS profiles below and above the melting temperatures of the crystals are identical, indicating that the crystals are confined within the block copolymer domains. The conductivities of SEO/LiTFSI mixtures with $r = 0.275$, $r = 0.300$, and $r = 0.350$ are within experimental error of PEO/LiTFSI at the same salt concentrations, in spite of the presence of insulating polystyrene (PS) domains in the SEO/LiTFSI samples. We attribute this to enhanced segmental dynamics of the PEO chains in the SEO electrolytes, based on differential scanning calorimetry (DSC) measurements of glass transition temperatures. The dependence of ionic conductivity on salt concentration in the SEO/LiTFSI electrolytes at temperatures above the melting temperature of the crystalline complexes shows three local maxima that correlate with the formation of crystalline complexes when $r \geq 0.125$. These maxima arise due to a combination of the enhanced segmental dynamics and changes in morphology observed by SAXS and STEM.
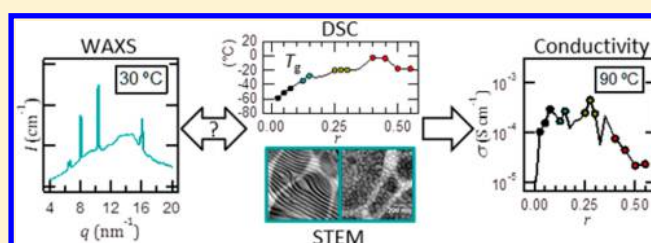
INTRODUCTION

Block copolymer electrolytes have garnered significant interest due to their unique ability to decouple mechanical properties from electrochemical performance through microphase separation and self-assembly.[1] It has been predicted[2] and experimentally verified[3−6] that the mechanical properties of an electrolyte separator can influence the formation and propagation of "dendritic" structures that can short-circuit a battery cell. Developing a mechanically rigid electrolyte that maintains suitable electrochemical properties represents a promising route toward enabling next-generation batteries that utilize high energy density metal foil anodes (e.g., the lithium metal anode).

The most well-studied block copolymer electrolyte system consists of the block copolymer polystyrene-*b*-poly(ethylene oxide) (SEO) mixed with a lithium salt.[7−10] Mixtures of SEO and lithium salts microphase-separate into nanoscale poly-

styrene-rich (PS) domains, which provide mechanical rigidity, and poly(ethylene oxide)-rich (PEO) domains, which solvate and conduct the lithium salt ions. Lithium bis(trifluoro-methanesulfonyl)imide has been the most commonly used salt in block copolymer electrolyte studies. In the SEO/LiTFSI system, ionic conductivity has been characterized as a function of SEO molecular weight,[11,12] block architecture,[13−15] end-group chemistry,[16,17] morphology,[16−18] and salt concentration.[11,19,20] It is convenient to express salt concentration in terms of $r \equiv [\text{Li}]/[\text{EO}]$, the ratio of lithium (Li) to ethylene oxide (EO) moieties. Most studies on block copolymer electrolytes are centered around $r = 0.10$ as this is the regime wherein the conductivity of homopolymer PEO/LiTFSI

electrolytes is maximized.[21] Chintapalli et al.[19] investigated the ionic conductivity of two moderate molecular weight SEOs mixed with LiTFSI up to $r = 0.55$. The two copolymers were called SEO(16−16) and SEO(4.9−5.5), where the numbers in parentheses indicate the molecular weights of the PS and PEO blocks in kg mol^{-1}. In that study, both systems exhibited a lamellar morphology in the salt concentration range of interest, and surprisingly, the global maximum in ionic conductivity of both polymers occurred at $r = 0.21$,[19] a factor of 2 larger than the value of r at which the maximum is observed in homopolymer PEO/LiTFSI.[21] The higher conductivity of SEO/LiTFSI in the high salt concentration limit was attributed to a salt-induced increase in morphological disorder (i.e., reduced grain sizes).[19] This can be rationalized by noting that salt ions tend to cause associations between segments of single and neighboring PEO chain, which in turn hinders the formation of equilibrated lamellae with long-range order.

The purpose of this work is to report on the relationship between morphology and ionic conductivity in block copolymer electrolytes derived from a high molecular weight SEO [SEO(52−55)] mixed with LiTFSI at salt concentrations of $0 \leq r \leq 0.55$. We are mainly interested in morphology and ionic conductivity above the melting point of the PEO-rich microphase. The ionic conductivity of the SEO(52−55)/LiTFSI electrolytes exhibit three maxima with increasing salt concentration. We present results of characterization experiments [small- and wide-angle X-ray scattering (SAXS/WAXS), scanning transmission electron microscopy (STEM), and differential scanning calorimetry (DSC)] aimed at explaining this observation.

■ EXPERIMENTAL SECTION

Materials. The polystyrene-*b*-poly(ethylene oxide) (SEO) diblock copolymer used in this study was synthesized using sequential anionic polymerization, as described in refs 22, 23, and 12. Details about the purification and characterization can be found in the Supporting Information. The polymer has the following characteristics: $M_{n,PS} = 52$ kg mol^{-1}, $M_{n,PEO} = 55$ kg mol^{-1}, PDI = 1.1, and $\phi_{PEO} = 0.50$ at 90 °C.[24] We will refer to the polymer as SEO(52−55) for the remainder of this work. The polymer was dried under vacuum at 90 °C for 24 h before being stored in an argon-filled glovebox (MBraun) with sub-ppm water and oxygen levels. Lithium bis(trifluoromethanesulfonyl)-imide (LiTFSI) was obtained from Novolyte. The LiTFSI container was opened inside of the glovebox and then dried in a heated antechamber under vacuum for 3 days at 120 °C before use.

The block copolymer electrolytes used in this study were prepared in the same manner as ref 19 by mixing solutions of SEO(52−55)/benzene (∼1 wt %) and LiTFSI/THF (18−30 wt %) in ratios that provided the targeted electrolyte salt concentration. In total, 20 solutions were prepared with salt concentrations ranging from $r = 0.000$ (neat) to $r = 0.550$, where $r \equiv [\text{Li}]/[\text{EO}]$ is the ratio of lithium to ethylene oxide (EO) moieties. The solutions were subsequently lyophilized in a Millrock LD85 lyophilizer using a custom air-free transfer stage. The lyophilized samples were transferred back into the glovebox antechamber and dried under vacuum for 12 h at 90 °C before use. All subsequent sample preparation was performed within the argon glovebox.

Small- and Wide-Angle X-ray Scattering (SAXS/WAXS). The lyophilized SEO(52−55)/LiTFSI block copolymer electrolyte samples were generally fluffy white powders, although at the highest salt concentrations they formed a more dense porous solid. X-ray scattering samples were prepared by packing the SEO(52−55)/LiTFSI powder into 1/8 in. inner diameter spacer made of chemically resistant and thermally stable Aflas rubber. The polymer-filled spacer was placed between two sheets of fluorinated ethylene−propylene (FEP) Teflon and hot pressed at ∼130 °C with a hand-held press.

After several rounds of adding polymer and hot-pressing, the Aflas spacer was filled with a solid disc of electrolyte. The block copolymer electrolyte/spacers were then covered on both sides with 1 mil Kapton films and assembled into custom hermetically sealed aluminum sample holders. An empty sample was also prepared using the same protocol for use as a blank reference during the scattering measurements. The hermetically sealed samples (including the blank) were removed from the glovebox and annealed under vacuum at 140 °C for 1 week. After annealing, the oven heater was turned off and the samples were allowed to slowly cool in a nitrogen-purged atmosphere at −6 mmHg for 72 h.

X-ray scattering measurements were performed in transmission geometry at the Advanced Light Source (ALS) Beamline (BL) 7.3.3[25] and the Stanford Synchrotron Radiation Laboratory (SSRL) BL 1-5 using a custom heating stage designed to hold the hermetically sealed aluminum sample holders. Each experiment was replicated using first a small-angle (SAXS) configuration, and then a wide-angle (WAXS) setup [the samples were reannealed for 24 h and allowed to slowly cool for 72 h, as described above, between SAXS and WAXS experiments]. SAXS from SEO(52−55)/LiTFSI samples with $r = 0.000−0.350$ were measured using an ∼3.8 m detector distance, 10 keV X-rays, and a Pilatus 2M (Dectris) detector at ALS BL 7.3.3, while SAXS from SEO(52−55)/LiTFSI samples with $r = 0.400−0.550$ were measured at SSRL BL 1-5 using an ∼3 m detector distance, 10 keV X-rays, and a Rayonix 165 CCD camera. All WAXS measurements were performed at ALS 7.3.3 using an ∼0.3 m detector distance, 10 keV X-rays, and the Pilatus 2M detector. In all cases, the actual sample-to-detector distance (SD) was determined from the scattering pattern of a silver behenate (AgB) calibration standard.

Each scattering experiment followed the same general protocol. First, the scattering for each sample was measured at 30 °C. The sample stage was then heated directly to 70 °C, where samples were allowed to equilibrate for at least 40 min before recording any scattering measurements. From 70 °C, a heating scan was performed in 10 °C intervals up to 120 °C, waiting at least 30 min at each temperature before making measurements. The samples were held for an additional 30 min at 120 °C to ensure the samples were equilibrated. When beamtime was available, a subsequent cooling scan was performed back down to 70 °C. It was found during these experiments that sample structure had a slight temperature dependence during heating but was essentially temperature-independent upon cooling. Thus, in order to compare all of the samples, only the scattering results from 30 °C (after controlled annealing) and 120 °C will be discussed in this work. After the final scattering measurements, the samples were returned to the glovebox and were disassembled in order to measure each sample thickness.

The 2D scattering images were processed using the Nika[26] macro in Igor Pro. 1D intensity (I) versus q profiles were obtained by azimuthally averaging the images; $q \equiv \frac{4\pi}{\lambda} \sin\left(\frac{\theta}{2}\right)$ represents the magnitude of the scattering vector, where λ is the X-ray wavelength and θ is the scattering angle. The 1D profiles were corrected for sample attenuation and scattering from the blank reference as described previously.[27] All corrected intensity profiles were then calibrated to absolute units using the scattering from a glassy carbon reference[28] (sample M13, obtained from Jan Ilavsky).

Scanning Transmission Electron Microscopy (STEM). For selected electrolyte concentrations, the second half of the X-ray scattering sample (not used for thermal analysis) was further analyzed using STEM. These bulk electrolyte pieces were cryo-microtomed at −90 °C in a Leica FC6. Sections with thicknesses of approximately 100 nm were obtained using a diamond knife and picked up onto lacey carbon-coated copper grids (Electron Microscopy Sciences). STEM samples were stained in ruthenium tetroxide vapor for 30 min prior to experiments. STEM experiments were performed on an FEI Titan microscope operated at 200 kV at the National Center for Electron Microscopy of the Molecular Foundry, Lawrence Berkeley National Lab. The microscope is equipped with a high angle annular dark field detector (HAADF).

Thermal Analysis. After the scattering measurements, the thermal properties for each SEO(52−55)/LiTFSI sample were measured using differential scanning calorimetry (DSC). About half (3−6 mg) of each X-ray scattering sample was placed in a TZero aluminum pan and sealed with a TZero hermetic lid (T.A. Inc.) inside of the argon glovebox. The samples were removed from the glovebox and reannealed in the vacuum oven for 24 h before being slowly cooled and allowed to sit at room temperature for 72 h, as described earlier. The thermal properties of the samples were then measured using a heat-quench-heat method: the samples were equilibrated at 30 °C, heated at 5 °C/min up to 130 °C, held isothermally for 20 min, quenched to −80 °C, and then heated back up to 130 °C at 10 °C/min. Analysis was performed using the TA Instruments Universal Analysis 2000 software: melting transitions were analyzed from the first heating scan using the "Peak Integrate Linear" function, while glass transitions were analyzed from the second heating scan using the "Glass/Step Transition" function. Melting temperatures (T_m's) are reported from the peak temperature values, and glass transition temperatures (T_g's) are taken as the inflection temperature during the glass transition.

Electrochemical Characterization. The ionic conductivity (σ) of each SEO(52−55)/LiTFSI electrolyte was measured in triplicate. Samples were prepared by placing pellet of the lyophilized SEO(52−55)/LiTFSI sample in the center of a fiberglass spacer (Garolite G10, 5 mil thickness) with an inner diameter of 6.35 mm. The polymer-filled spacer was placed between two sheets of FEP Teflon and pressed in a pneumatic hot press at 130 °C and 40 psi for 30 s. The sample was subsequently flipped and pressed again to achieve a uniform polymer disc within the G10 spacer. Pieces of 0.0175 mm thick electrode-grade aluminum foil were placed on both sides of the polymer-filled spacer to serve as electrodes. The sample was hot pressed again at 130 °C and 40 psi for 30 s to ensure good contact between the electrodes and the block copolymer electrolyte. The thickness of each sample was measured using a micrometer, and then aluminum current collector tabs were placed on the electrodes and the cell was vacuum sealed in an air-free pouch material (Showa Denko).

The ionic conductivities were determined using potentiostatic electrochemical impedance spectroscopy (PEIS) and the sample geometry. PEIS measurements were made using a Biologic VMP3 potentiostat. Sample temperature was maintained using a custom-built programmable heating stage. During each experiment, the as-prepared samples were initially heated to and held isothermally at 130 °C for 3 h. Subsequently, their impedance was measured at 130 °C, and then a cooling scan to 70 °C was performed with 10 °C increments. The samples were held at each temperature for 1 h before measurement. The PEIS measurements utilized a 50 mV excitation voltage with a frequency range from 1 MHz to 1 Hz. The dc resistance (R) of the electrolyte was determined from a Bode plot of the data, where it was interpreted as the impedance value on the bode plateau at the frequency where the maximum phase angle was observed. After PEIS measurements, the samples were disassembled in order to measure their final thickness. Ionic conductivity (σ) was then calculated from $\sigma = L/RA$, where L is the sample thickness, R is the dc resistance, and A is the sample area.

■ RESULTS AND DISCUSSION

The combined SAXS/WAXS profiles for all 20 SEO(52−55)/LiTFSI block copolymer electrolytes at room temperature (after thermal pretreatment) are presented in Figure 1. Each SAXS and WAXS curve are provided in absolute scattering intensity from independent intensity calibrations; offsets between SAXS and WAXS curves of the same sample are likely due to parasitic background intensity in the high-q portion of the SAXS data and errors in the sample thickness normalization.[27] In Figure 1a, it is evident that neat SEO (r = 0.00) exhibits poor long-range order. On the basis of the composition and molecular weight of the block copolymer, we would expect a lamellar morphology with sharp interfaces. A
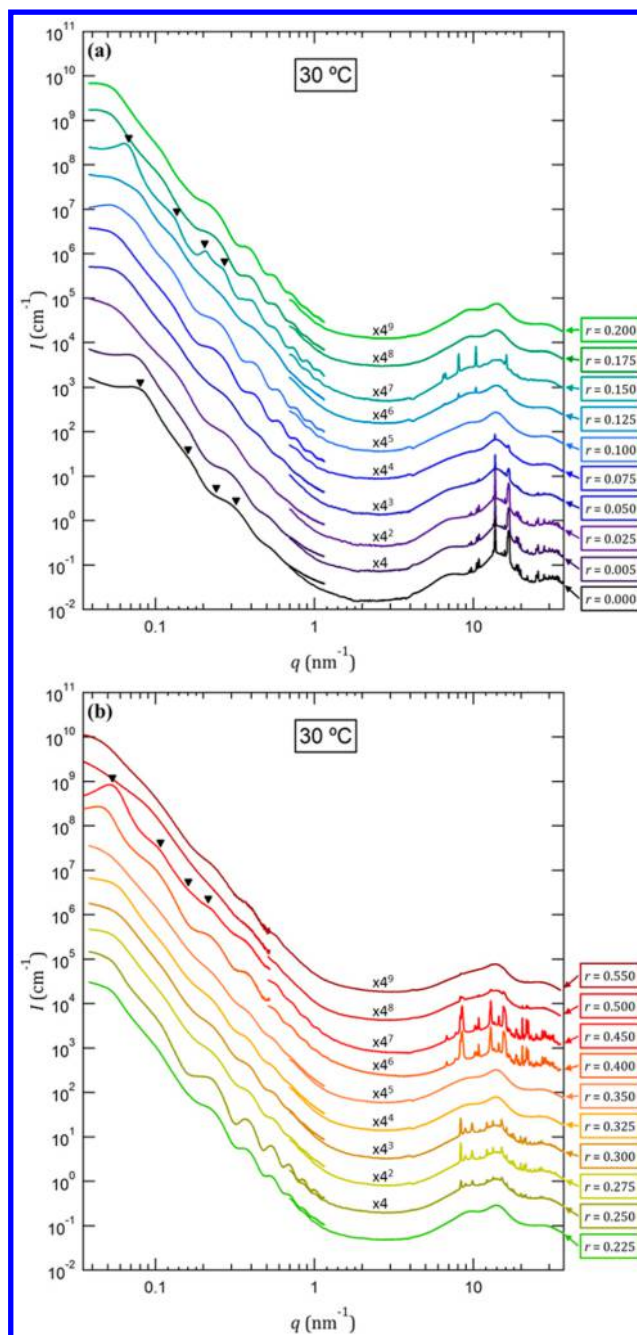

Figure 1. Combined SAXS/WAXS profiles for the SEO(52−55)/LiTFSI electrolytes at 30 °C for (a) r = 0−0.200 and (b) r = 0.250−0.550. Each salt concentration is indicated by a data tag. Intensities are absolute, but offset by the factors indicated on the plot for clarity. Filled upside-down triangles represent the expected peak positions for a lamellar morphology.

weak SAXS maximum is seen at $q = q^* = 0.08$ nm^{-1}, indicating that the center-to-center distance between adjacent PEO lamellae is $d = 2\pi/q^* = 79$ nm. This is in excellent agreement with the correlation presented in ref 11, d (nm) = 3.15 $M^{0.69}$, where M is the total molecular weight of the SEO copolymer in kg mol^{-1}, which yields d = 80 nm. The expected higher order peaks, shown by triangles in Figure 1, are not prominent, but weak shoulders are evident at some of the expected locations. The WAXS profile for neat SEO displays clear evidence of crystalline PEO domains. As the LiTFSI concentration is

increased from $r = 0.00$ to $r = 0.100$, the primary SAXS maximum in the vicinity of $q* = 0.08$ nm^{-1} is reduced to a shoulder, and oscillations at high q typically associated with the form factor scattering of dispersions[29] are evident. As the LiTFSI concentration is increased from $r = 0.00$ to $r = 0.100$, there is also a decrease in WAXS peak intensity, indicating a decrease in PEO crystallinity. At $r = 0.125$ this trend is disrupted, and new WAXS peaks emerge. Increasing the LiTFSI concentration to $r = 0.150$ causes the development of a well-defined SAXS peak at $q* = 0.07$ nm^{-1} with the expected higher order peaks for a lamellar morphology. Simultaneously, the intensity of the WAXS peaks increase. The WAXS peaks in the range $r = 0.125-0.150$ are consistent with the diffraction from the crystalline "C_6" PEO−LiTFSI complex, where each lithium ion is associated with six EO units.[21,30−32] Further increasing the salt concentration results in the disappearance of all WAXS peaks and the reemergence of the decaying SAXS oscillations for the range of $r = 0.175-0.225$ (Figure 1a,b). At $r = 0.250$, the appearance of new WAXS peaks indicates the presence of the crystalline "C_3" PEO−LiTFSI complex.[21,31,33,34] In this case, no Bragg peaks are observed in the SAXS profile; however, the decaying oscillations become more clearly defined. The C_3 complex persists through $r = 0.300$, but the oscillations in SAXS appear damped with increasing LiTFSI concentration. WAXS peaks associated with the "C_2" PEO−LiTFSI complex[21,31,35] appear at $r = 0.400$ and remain prominent at $r = 0.450$, where the SAXS profile again indicates the presence of periodic order. The lack of defined higher order SAXS peaks precludes the assignment of the morphology at $r = 0.450$. Increasing LiTFSI concentration beyond $r = 0.450$ results in a decrease of C_2 crystallinity, and the SAXS signatures of periodic order are lost.

The SAXS/WAXS data obtained at elevated temperatures (120 °C) are shown in the Supporting Information (Figure S4). Aside from the melting of the PEO/LiTFSI crystals and a concomitant reduction in absolute intensity due to changes in scattering contrast, there are no differences between the data obtained at 120 and 30 °C. It is evident the morphology of our electrolytes on length scales commensurate with the domain spacing is independent of temperature, an expected result given the glassy nature of the microphase-separated PS domains.[36]

Motivated by the atypical SAXS profiles portrayed in Figure 1, we selected a number of samples to image using STEM. Figure 2a shows the morphology of neat SEO where bright regions indicate the PEO-rich domains. The sample lacks long-range periodic order; local regions of lamellar-like packing coexist with ellipsoidal PEO-rich domains that are surrounded by PS-rich layers. These ellipsoidal domains are the predominant structural motif at $r = 0.100$ (Figure 2b). The STEM data suggest that the decaying oscillations in the SAXS profile at $r = 0.100$ in Figure 1a arise from form factor scattering of the ellipsoidal domains. The sample at $r = 0.150$ (Figure 2c) presented an interesting morphology that was different from the samples at lower salt concentrations. Here we see two distinct regions: some regions contained the poorly ordered ellipsoids, but others contained classical lamellae with smooth undulations. Increasing salt concentration to $r = 0.450$ resulted in a uniform morphology with undulating lamellae seen at all locations. Given the extensive annealing protocol that was applied to all of the samples, the observation of nonlamellar morphologies in Figures 1 and 2, especially in the salt-free SEO(52−55) sample, indicates that self-assembly in the melt is kinetically limited in this system.
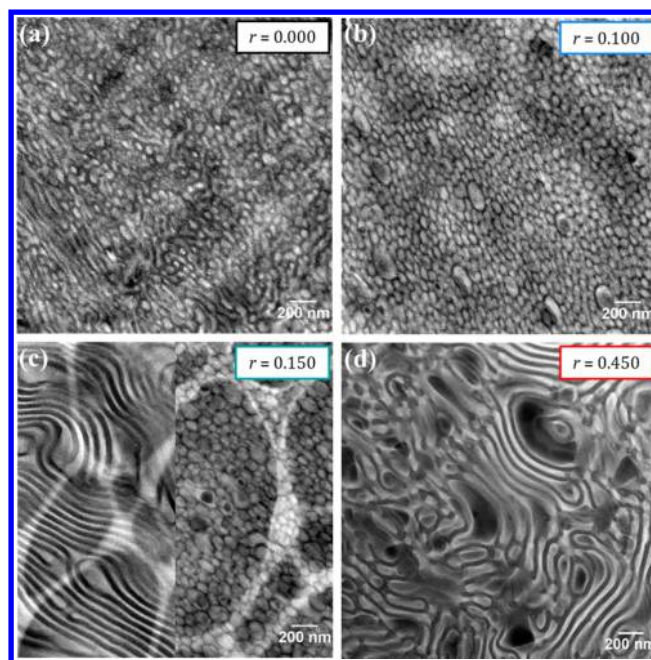
Figure 2. STEM micrographs of selected electrolyte concentrations. (a) SEO(52−55)/LiTFSI($r = 0.000$); (b) SEO(52−55)/LiTFSI($r = 0.100$); (c) SEO(52−55)/LiTFSI($r = 0.150$); and (d) SEO(52−55)/LiTFSI($r = 0.450$). Bright regions indicate PEO-rich phases. The micrograph in (c) is a composite of two separate images taken from difference regions of the sample; the scale bar applies to both images. The support used to hold the sample is visible in (c).

In Figure 3a, we plot the DSC-determined melting temperatures (T_m's) of PEO and PEO−LiTFSI crystalline complexes for the SEO(52−55)/LiTFSI samples, along with the data from homopolymer PEO/LiTFSI reported by Lascaud et al.;[21] the data markers of samples that exhibited WAXS peaks are highlighted to indicate the crystal structure observed. In addition to the crystalline melting data, we also include the DSC-determined glass transition temperature for polystyrene ($T_{g,PS}$) for each SEO(52−55)/LiTFSI sample. The polystyrene T_g is unaffected by salt addition, indicating that the salt mainly resides in the PEO domains. As shown in Figure 3a, the T_m for crystalline PEO is depressed as the LiTFSI concentration is increased from $r = 0.000$ to 0.075. This is a manifestation of freezing point depression. At $r = 0.100$, all PEO crystallization is suppressed and no melting transition is detected by DSC, consistent with the lack of WAXS peaks for that sample. At $r = 0.125$, a thermal transition is observed in DSC, which we can unambiguously attribute to the melting of the C_6 complex observed in WAXS. As more salt is added, the T_m for the C_6 complex goes through a maximum, and then all crystallization is disrupted at $r = 0.200$. The melting transitions for $0.250 \leq r \leq 0.300$ are due to the melting of the C_3 complex. Increasing the LiTFSI content to $r = 0.400$ results in the observation of the C_2 complex. This complex persists up to $r = 0.550$. In the narrow concentration window between the C_3 and C_2 complexes, $0.325 \leq r \leq 0.350$, two thermal transitions are observed in DSC. We posit the presence of coexisting C_3 and C_2 complexes in these samples, in spite of the absence of detectable WAXS peaks. Overall, Figure 3a indicates that the crystallization behavior in SEO(52−55)/LiTFSI (filled symbols in Figure 3a) is similar to that of PEO/LiTFSI (open symbols in Figure 3a). Furthermore, in the Supporting Information (SI 2) we show
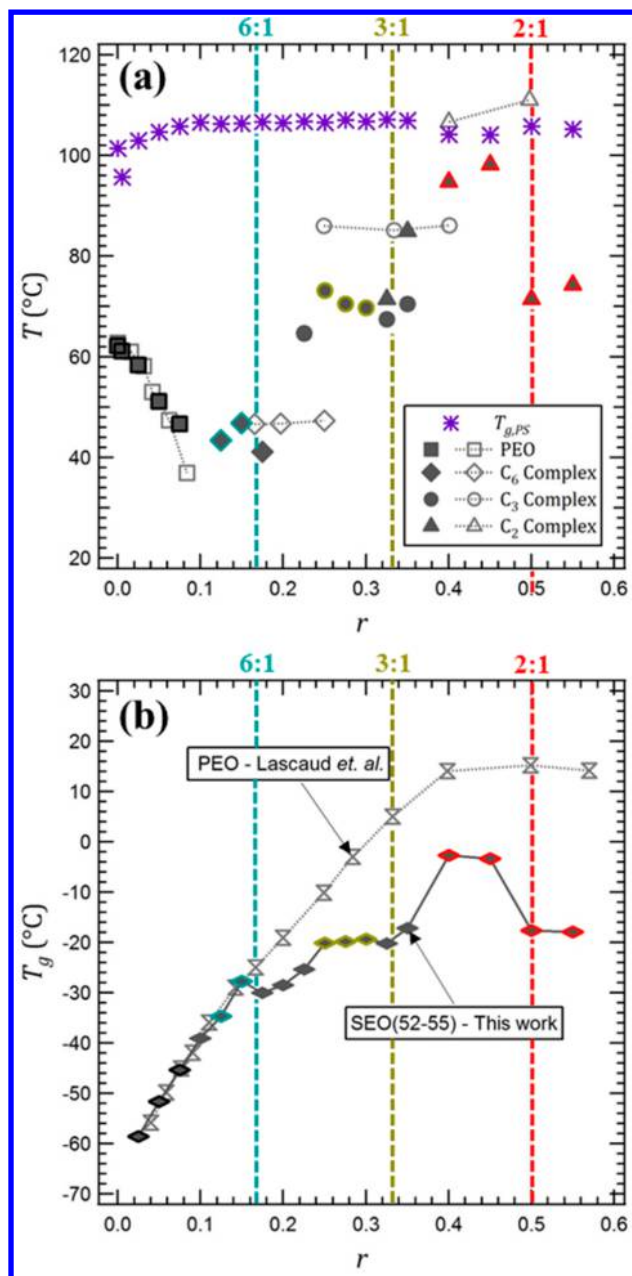
Figure 3. (a) Phase diagram for PEO/LiTFSI determined from DSC and WAXS, along with the DSC-measured PS glass transition temperatures ($T_{g,PS}$, purple stars) for reference. Filled symbols represent the data from this work, while open symbols connected with dashed lines correspond to the data from Lascaud et al.[21] Melting transitions from different crystal structures are represented by symbol shape: squares = pure PEO crystals; diamonds = the C_6 complex; circles = the C_3 complex; and triangles = the C_2 complex. (b) PEO-phase glass transition temperatures determined by DSC. Filled diamonds connected with solid lines represent the data from this work, while open hourglasses connected with dashed lines correspond to the data from Lascaud et al.[21] In both plots, block copolymer electrolyte samples that demonstrated crystalline WAXS peaks are indicated with a highlight color: black = pure PEO; turquoise = C_6 complex; earth-green = C_3 complex; and red = C_2 complex. Dashed vertical lines with the same highlight colors are used to indicate the stoichiometric concentration for each PEO−LiTFSI crystal complex.

that the crystal structures observed for PEO/LiTFSI and SEO(52−55)/LiTFSI are identical.

Ion transport in amorphous PEO-rich domains depends on segmental dynamics, which is related to the T_g.[21] Figure 3b plots T_g as a function of salt concentration for PEO/LiTFSI and SEO(52−55)/LiTFSI. Increasing salt concentration has been shown to inhibit segmental mobility in PEO[37−40] due to the formation of ion-induced transient physical cross-links. This is clearly seen in the PEO/LiTFSI data where the T_g increases monotonically with salt concentration until it appears to saturate at $r = 0.40$. Interestingly, the T_g for the PEO-rich phase of the SEO(52−55)/LiTFSI samples matches that of PEO/LiTFSI for $r \leq 0.150$ but is significantly lower at all higher salt concentrations. Furthermore, unlike the near linear increase observed for PEO/LiTFSI, the T_g values from the block copolymer electrolyte samples show multiple plateaus when the salt concentration is increased above $r = 0.150$. These plateaus imply that the traditional slowing down of segmental motion due to salt addition seen in homopolymers may not be applicable to block copolymers. Interestingly, each plateau in T_g appears to be related to the PEO−LiTFSI crystalline complexes. For example, the T_g plateau observed for $0.250 \leq r \leq 0.325$ encompasses all concentrations wherein the C_3 complex forms. We posit that segmental dynamics and ion−polymer interactions are affected by chain stretching[9,41] due to the attachment of PEO to the glassy PS domains and that these factors depend on the microphase-separated morphology.

The dependence of ionic conductivity on salt concentration in SEO(52−55)/LiTFSI and PEO/LiTFSI at 90 °C is compared in Figure 4. The PEO/LiTFSI data show a single maximum in ionic conductivity at $r = 0.100$. In contrast, the
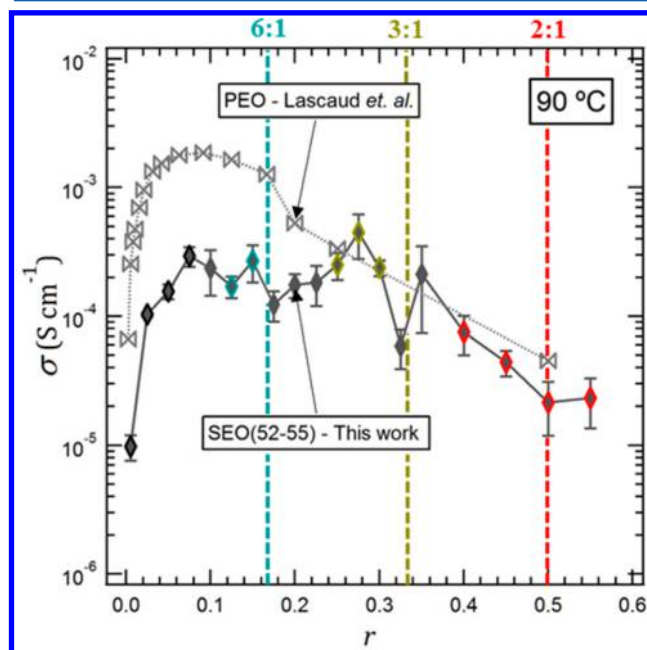
Figure 4. Ionic conductivity of the SEO(52−55)/LiTFSI samples (filled diamonds, solid lines) from this work and for PEO from Lascaud et al.[21] (open horizontal hourglass, dashed lines) as a function of salt concentration at 90 °C. Error bars represent the standard deviation in the average of at least three replicate samples. SEO(52−55)/LiTFSI samples that demonstrated crystalline WAXS peaks are indicated with a highlight color: black = pure PEO; turquoise = C_6 complex; earth-green = C_3 complex; and red = C_2 complex. Dashed vertical lines with the same highlight colors are used to indicate the stoichiometric concentration for each PEO−LiTFSI crystal complex.

relationship between salt concentration and ionic conductivity in SEO(52−55)/LiTFSI electrolytes is much more complex. There are two observations that deserve explanation: [1] the concentration dependence of conductivity in SEO(52−55)/LiTFSI is jagged, with three maxima in the vicinity of $r = 0.075$, $r = 0.275$, and $r = 0.350$, and [2] the conductivities of SEO(52−55)/LiTFSI at $r = 0.275$, $r = 0.300$, and $r = 0.350$ are within experimental error of those for PEO/LiTFSI, despite the presence of insulating PS domains.

Effective medium theory[42] indicates that for a microphase-separated sample with one conducting phase, the ionic conductivity at a given salt concentration, $\sigma(r)$, is described by[11]

$$\sigma(r) = f\phi_c\sigma_c(r) \qquad (1)$$

where f is the morphology factor that accounts for the geometry and connectivity of the conducting phase, ϕ_c is the volume fraction of the conducting phase, and $\sigma_c(r)$ is the intrinsic conductivity of conducting phase, which is typically approximated by the conductivity of PEO/LiTFSI at the salt concentration of interest. By definition, $f \leq 1$, and for a randomly oriented lamellar morphology, $f = 2/3$.[11,42] It is clear that simple application of effective medium theory provides no explanation for the two observations listed above: [1] the theory indicates that the numbers of maxima observed in block copolymer and homopolymer electrolytes must be identical, and [2] the conductivity of the block copolymer electrolyte must always be lower than that of the homopolymer electrolyte.

The data presented in Figures 1−3 suggest rational explanations for the two anomalies listed above. [1] The unexpected maxima in SEO(52−55)/LiTFSI conductivity for $r > 0.100$ appear to correlate with the changes in morphology observed in Figures 1 and 2. Although the salt-induced crystals are not present during the conductivity measurements, changes in the morphology factor, f, associated with crystallization in Figure 1 affect the conductivity. [2] At salt concentrations where the conductivity of SEO(52−55)/LiTFSI is comparable to homopolymer PEO/LiTFSI, the glass transition temperature of the PEO-rich microphase in SEO(52−55) is significantly (∼15 °C) lower than that of PEO/LiTFSI (see Figure 3b). A reduced T_g implies an increased mobility of the PEO segments, which is known to increase the conductivity of the PEO-rich microphase,[40] $\sigma_c(r)$.

CONCLUSIONS

Characterization of SEO(52−55)/LiTFSI mixtures over a wide salt concentration range ($0.00 \leq r \leq 0.55$) has revealed phenomena not previously observed in the field of block copolymer electrolytes:

(1) At some salt concentrations, the conductivity is within experimental error of the conductivity of PEO/LiTFSI, in spite of the presence of insulating PS-rich domains in the SEO-based electrolytes (Figure 4 and Figure S7). DSC experiments show that T_g corresponding to the PEO-rich microphases in the SEO electrolyte is lower than that of the homopolymer PEO/LiTFSI mixtures (Figure 3b) at those salt concentrations; the lower T_g indicates faster segmental dynamics relative to homopolymer PEO/LiTFSI, which could provide the observed increase in conductivity.

(2) Conventional wisdom suggests that increasing salt concentration in polymer electrolytes increases charge

carrier concentration but slows down segmental motion. In the absence of morphological changes, one would expect one maximum in conductivity as a function of salt concentration, as is usually observed in amorphous polymer electrolytes. In contrast, the conductivity of amorphous SEO electrolytes exhibits three local maxima as a function of salt concentration (Figure 4). One contributing factor is the fact that T_g of SEO/LiTFSI mixtures does not increase smoothly with increasing salt concentration (Figure 3b). The conductivity maxima observed for $r > 0.100$ appear to correlate with the changes in morphology observed by SAXS (Figure 1), which in turn are associated with the formation of salt-induced crystalline complexes (C_6, C_3, and C_2). Salt-induced crystallization impacts conductivity, even though the crystals are not present during the conductivity measurements, because it affects the microphase-separated morphology (Figure 1 and Figure S4).

This work shows that the relationship between morphology, ion−polymer interactions, and conductivity in high molecular weight block copolymer electrolytes is more complex that previous studies suggest.

ASSOCIATED CONTENT

Ⓢ Supporting Information

The Supporting Information is available free of charge on the ACS Publications website at DOI: 10.1021/acs.macromol.7b02415.

> SI 1: details about the purification and characterization of SEO(52−55); SI 2: SAXS/WAXS analysis of SEO(52−55)/LiTFSI electrolytes at elevated temperatures, as well as the detailed WAXS profiles for each PEO crystalline structure; SI 3: the temperature-dependent ionic conductivity results from all SEO(52−55)/LiTFSI electrolytes and their comparison with PEO/LiTFSI at 130 °C (PDF)

AUTHOR INFORMATION

Corresponding Author
*E-mail: nbalsara@berkeley.edu (N.P.B.).

ORCID Ⓘ
Jacob L. Thelen: 0000-0003-0026-4404
X. Chelsea Chen: 0000-0003-1188-7658
Nitash P. Balsara: 0000-0002-0106-5565

Notes
The authors declare no competing financial interest.

ACKNOWLEDGMENTS

■ NOMENCLATURE

Abbreviations

DSC	differential scanning calorimetry
C_2	2:1 (PEO:LiTFSI) crystal complex
C_3	3:1 (PEO:LiTFSI) crystal complex
C_6	6:1 (PEO:LiTFSI) crystal complex
EO	ethylene oxide
FEP	fluorinated ethylene propylene
LiTFSI	lithium bis(trifluoromethanesulfonyl)imide
PDI	polydispersity index
PEIS	potentiostatic electrochemical impedance spectroscopy
PEO	poly(ethylene oxide)
PS	polystyrene
SAXS	small-angle X-ray scattering
SEO	polystyrene-*b*-poly(ethylene oxide) diblock copolymer
STEM	scanning transmission electron microscopy
THF	tetrahydrofuran
WAXS	wide-angle X-ray scattering

Symbols

A	electrode area in conductivity cells, cm^2
f	morphology factor
I	absolute scattering intensity, cm^{-1}
L	electrode thickness in conductivity cell, cm
$M_{n,PEO}$	number-average molecular weight of the PEO block, kg mol^{-1}
$M_{n,PS}$	number-average molecular weight of the PS block, kg mol^{-1}
q	magnitude of the scattering vector, nm^{-1}
r	salt concentration [Li$^+$][EO]$^{-1}$
R	dc resistance of the electrolyte, Ω
T_g	glass transition temperature, °C
$T_{g,PS}$	glass transition temperature of polystyrene, °C
T_m	melting temperature, °C

Greeks

ϕ_c	volume fraction of the conducting phase
λ	scattering radiation wavelength, nm
θ	scattering angle, rad
σ	ionic conductivity, S cm^{-1}
$\sigma_c(r)$	intrinsic ionic conductivity of the conducting phase, S cm^{-1}

■ REFERENCES

(1) Singh, M.; Odusanya, O.; Wilmes, G. M.; Eitouni, H. B.; Gomez, E. D.; Patel, A. J.; Chen, V. L.; Park, M. J.; Fragouli, P.; Iatrou, H.; et al. Effect of Molecular Weight on the Mechanical and Electrical Properties of Block Copolymer Electrolytes. *Macromolecules* **2007**, *40*, 4578–4585.

(2) Monroe, C.; Newman, J. The Impact of Elastic Deformation on Deposition Kinetics at Lithium/Polymer Interfaces. *J. Electrochem. Soc.* **2005**, *152*, A396.

(3) Harry, K. J.; Higa, K.; Srinivasan, V.; Balsara, N. P. Influence of Electrolyte Modulus on the Local Current Density at a Dendrite Tip on a Lithium Metal Electrode. *J. Electrochem. Soc.* **2016**, *163*, A2216–A2224.

(4) Hallinan, D. T.; Mullin, S. A.; Stone, G. M.; Balsara, N. P. Lithium Metal Stability in Batteries with Block Copolymer Electrolytes. *J. Electrochem. Soc.* **2013**, *160*, A464–A470.

(5) Schauser, N. S.; Harry, K. J.; Parkinson, D. Y.; Watanabe, H.; Balsara, N. P. Lithium Dendrite Growth in Glassy and Rubbery Nanostructured Block Copolymer Electrolytes. *J. Electrochem. Soc.* **2015**, *162*, A398–A405.

(6) Khurana, R.; Schaefer, J. L.; Archer, L. A.; Coates, G. W. Suppression of Lithium Dendrite Growth Using Cross-Linked Polyethylene/Poly(ethylene Oxide) Electrolytes: A New Approach for Practical Lithium-Metal Polymer Batteries. *J. Am. Chem. Soc.* **2014**, *136*, 7395–7402.

(7) Young, W.-S.; Kuan, W.-F.; Epps, T. H. Block Copolymer Electrolytes for Rechargeable Lithium Batteries. *J. Polym. Sci., Part B: Polym. Phys.* **2014**, *52*, 1–16.

(8) Young, W.; Epps, T. H. Salt Doping in PEO-Containing Block Copolymers: Counterion and Concentration Effects. *Macromolecules* **2009**, *42*, 2672–2678.

(9) Young, W.; Epps, T. H. Ionic Conductivities of Block Copolymer Electrolytes with Various Conducting Pathways: Sample Preparation and Processing Considerations. *Macromolecules* **2012**, *45*, 4689–4697.

(10) Zardalidis, G.; Gatsouli, K.; Pispas, S.; Mezger, M.; Floudas, G. Ionic Conductivity, Self-Assembly, and Viscoelasticity in Poly(styrene-B-Ethylene Oxide) Electrolytes Doped with LiTf. *Macromolecules* **2015**, *48*, 7164–7171.

(11) Panday, A.; Mullin, S. A.; Gomez, E. D.; Wanakule, N. S.; Chen, V. L.; Hexemer, A.; Pople, J.; Balsara, N. P. Effect of Molecular Weight and Salt Concentration on Conductivity of Block Copolymer Electrolytes. *Macromolecules* **2009**, *42*, 4632–4637.

(12) Yuan, R.; Teran, A. A.; Gurevitch, I.; Mullin, S. A.; Wanakule, N. S.; Balsara, N. P. Ionic Conductivity of Low Molecular Weight Block Copolymer Electrolytes. *Macromolecules* **2013**, *46*, 914–921.

(13) Devaux, D.; Glé, D.; Phan, T. N. T.; Gigmes, D.; Giroud, E.; Deschamps, M.; Denoyel, R.; Bouchet, R. Optimization of Block Copolymer Electrolytes for Lithium Metal Batteries. *Chem. Mater.* **2015**, *27*, 4682–4692.

(14) Bates, C. M.; Chang, A. B.; Momčilović, N.; Jones, S. C.; Grubbs, R. H. ABA Triblock Brush Polymers: Synthesis, Self-Assembly, Conductivity, and Rheological Properties. *Macromolecules* **2015**, *48*, 4967–4973.

(15) Sarapas, J. M.; Saijo, K.; Zhao, Y.; Takenaka, M.; Tew, G. N. Phase Behavior and Li+ Ion Conductivity of Styrene-Ethylene Oxide Multiblock Copolymer Electrolytes. *Polym. Adv. Technol.* **2016**, *27*, 946–954.

(16) Jung, H. Y.; Mandal, P.; Jo, G.; Kim, O.; Kim, M.; Kwak, K.; Park, M. J. Modulating Ion Transport and Self-Assembly of Polymer Electrolytes via End-Group Chemistry. *Macromolecules* **2017**, *50*, 3224–3233.

(17) Jo, G.; Ahn, H.; Park, M. J. Simple Route for Tuning the Morphology and Conductivity of Polymer Electrolytes: One End Functional Group Is Enough. *ACS Macro Lett.* **2013**, *2*, 990–995.

(18) Teran, A. A.; Mullin, S. A.; Hallinan, D. T.; Balsara, N. P. Discontinuous Changes in Ionic Conductivity of a Block Copolymer Electrolyte through an Order−Disorder Transition. *ACS Macro Lett.* **2012**, *1*, 305–309.

(19) Chintapalli, M.; Le, T. N. P.; Venkatesan, N. R.; Mackay, N. G.; Rojas, A. A.; Thelen, J. L.; Chen, X. C.; Devaux, D.; Balsara, N. P. Structure and Ionic Conductivity of Polystyrene- Block -Poly(ethylene Oxide) Electrolytes in the High Salt Concentration Limit. *Macromolecules* **2016**, *49*, 1770–1780.

(20) Metwalli, E.; Rasool, M.; Brunner, S.; Müller-Buschbaum, P. Lithium-Salt-Containing High-Molecular-Weight Polystyrene- Block -Polyethylene Oxide Block Copolymer Films. *ChemPhysChem* **2015**, *16*, 2882–2889.

(21) Lascaud, S.; Perrier, M.; Vallee, A.; Besner, S.; Prud'homme, J.; Armand, M. Phase Diagrams and Conductivity Behavior of Poly-(ethylene Oxide)-Molten Salt Rubbery Electrolytes. *Macromolecules* **1994**, *27*, 7469−7477.

(22) Quirk, R. P.; Kim, J.; Kausch, C.; Chun, M. Butyllithium-Initiated Anionic Synthesis of Well-Defined Poly(styrene-Block-Ethylene Oxide) Block Copolymers with Potassium Salt Additives. *Polym. Int.* **1996**, *39*, 3−10.

(23) Hadjichristidis, N.; Iatrou, H.; Pispas, S.; Pitsikalis, M. Anionic Polymerization: High Vacuum Techniques. *J. Polym. Sci., Part A: Polym. Chem.* **2000**, *38*, 3211−3234.

(24) *Physical Properties of Polymers Handbook*; Mark, J. E., Ed.; Springer: New York, 2007.

(25) Hexemer, A.; Bras, W.; Glossinger, J.; Schaible, E.; Gann, E.; Kirian, R.; MacDowell, A.; Church, M.; Rude, B.; Padmore, H. A SAXS/WAXS/GISAXS Beamline with Multilayer Monochromator. *J. Phys. Conf. Ser.* **2010**, *247*, 012007.

(26) Ilavsky, J. Nika: Software for Two-Dimensional Data Reduction. *J. Appl. Crystallogr.* **2012**, *45*, 324−328.

(27) Thelen, J. L.; Chen, X. C.; Inceoglu, S.; Balsara, N. P. Influence of Miscibility on Poly(ethylene Oxide) Crystallization from Disordered Melts of Block Copolymers with Lithium and Magnesium Counterions. *Macromolecules* **2017**, *50*, 4827−4839.

(28) Zhang, F.; Ilavsky, J.; Long, G. G.; Quintana, J. P. G.; Allen, A. J.; Jemian, P. R. Glassy Carbon as an Absolute Intensity Calibration Standard for Small-Angle Scattering. *Metall. Mater. Trans. A* **2010**, *41*, 1151−1158.

(29) Roe, R.-J. *Methods of X-Ray and Nuetron Scattering in Polymer Science*; Oxford University Press: 2000.

(30) Marzantowicz, M.; Dygas, J. R.; Krok, F.; Nowiński, J. L.; Tomaszewska, A.; Florjańczyk, Z.; Zygadło-Monikowska, E. Crystalline Phases, Morphology and Conductivity of PEO:LiTFSI Electrolytes in the Eutectic Region. *J. Power Sources* **2006**, *159*, 420−430.

(31) Marzantowicz, M.; Dygas, J. R.; Krok, F.; Florjańczyk, Z.; Zygadło-Monikowska, E. Influence of Crystalline Complexes on Electrical Properties of PEO:LiTFSI Electrolyte. *Electrochim. Acta* **2007**, *53*, 1518−1526.

(32) Marzantowicz, M.; Dygas, J. R.; Krok, F.; Florjańczyk, Z.; Zygadło-Monikowska, E. Influence of Crystallization on Dielectric Properties of PEO:LiTFSI Polymer Electrolyte. *J. Non-Cryst. Solids* **2006**, *352*, 5216−5223.

(33) Andreev, Y. G.; Lightfoot, P.; Bruce, P. G. Structure of the Polymer Electrolyte Poly(ethylene oxide)3: LiN(SO2CF3)2 Determined by Powder Diffraction Using a Powerful Monte Carlo Approach. *Chem. Commun.* **1996**, 2169.

(34) Andreev, Y. G.; Bruce, P. G. Using Crystallography to Understand Polymer Electrolytes. *J. Phys.: Condens. Matter* **2001**, *13*, 8245−8255.

(35) Marzantowicz, M.; Krok, F.; Dygas, J. R.; Florjańczyk, Z.; Zygadło-Monikowska, E. The Influence of Phase Segregation on Properties of Semicrystalline PEO:LiTFSI Electrolytes. *Solid State Ionics* **2008**, *179*, 1670−1678.

(36) Zhu, L.; Cheng, S. Z. D.; Calhoun, B. H.; Ge, Q.; Quirk, R. P.; Thomas, E. L.; Hsiao, B. S.; Yeh, F.; Lotz, B. Crystallization Temperature-Dependent Crystal Orientations within Nanoscale Confined Lamellae of a Self-Assembled Crystalline - Amorphous Diblock Copolymer. *J. Am. Chem. Soc.* **2000**, *122*, 5957−5967.

(37) Mao, G.; Perea, R. F.; Howells, W. S.; Price, D. L.; Saboungi, M.-L. Relaxation in Polymer Electrolytes on the Nanosecond Timescale. *Nature* **2000**, *405*, 163−165.

(38) Mao, G.; Saboungi, M.; Price, D. L.; Armand, M.; Mezei, F.; Pouget, S. α-Relaxation in PEO−LiTFSI Polymer Electrolytes. *Macromolecules* **2002**, *35*, 415−419.

(39) Maranas, J. K. Solid Polymer Electrolytes. In *Dynamics of Soft Matter*; Sakai, V. G., Alba-Simionesco, C., Chen, S.-H., Eds.; Springer: New York, 2012; pp 123−143.

(40) Besner, S.; Prud'homme, J. Solvation Effect upon Glass Transition Temperature and Conductivity of Poly(ethylene Oxide) Complexed with Alkali Thiocyanates. *Macromolecules* **1989**, *22*, 3029−3037.

(41) Gomez, E. D.; Panday, A.; Feng, E. H.; Chen, V.; Stone, G. M.; Minor, A. M.; Kisielowski, C.; Downing, K. H.; Borodin, O.; Smith, G. D.; et al. Effect of Ion Distribution on Conductivity of Block Copolymer Electrolytes. *Nano Lett.* **2009**, *9*, 1212−1216.

(42) Sax, J.; Ottino, J. M. Modeling of Transport of Small Molecules in Polymer Blends: Application of Effective Medium Theory. *Polym. Eng. Sci.* **1983**, *23*, 165−176.